Evidence that protons act as neurotransmitters at vestibular hair cell–calyx afferent synapses

Stephen M. Highstein[a,1], Gay R. Holstein[b], Mary Anne Mann[a], and Richard D. Rabbitt[a,c,2]

[a]Marine Biological Laboratory, Woods Hole, MA 02543; [b]Department of Neurology, Icahn School of Medicine at Mount Sinai, New York, NY 10029; and [c]Department of Bioengineering, University of Utah, Salt Lake City, UT 84112

Present data support the conclusion that protons serve as an important neurotransmitter to convey excitatory stimuli from inner ear type I vestibular hair cells to postsynaptic calyx nerve terminals. Time-resolved pH imaging revealed stimulus-evoked extrusion of protons from hair cells and a subsequent buildup of $[H^+]$ within the confined chalice-shaped synaptic cleft ($\Delta pH \sim -0.2$). Whole-cell voltage-clamp recordings revealed a concomitant nonquantal excitatory postsynaptic current in the calyx terminal that was causally modulated by cleft acidification. The time course of $[H^+]$ buildup limits the speed of this intercellular signaling mechanism, but for tonic signals such as gravity, protonergic transmission offers a significant metabolic advantage over quantal excitatory postsynaptic currents—an advantage that may have driven the proliferation of postsynaptic calyx terminals in the inner ear vestibular organs of contemporary amniotes.

synaptic transmission | indefatigable

Information transmission in the nervous system occurs primarily through chemical signaling by small molecules packaged in synaptic vesicles and released quantally (1, 2) and gaseous free radicals that diffuse through 3D tissue volumes, oblivious to membrane boundaries (3–5). These two chemical modes of neurotransmission often act synergistically and in some systems, are augmented by electrical ephaptic interactions (6) and gap junctions (7). Here, we report a third mode of chemical intercellular signaling between inner ear type I hair cells and calyceal afferents: nonquantal protonergic transmission. Previously, proton release from the intestine during defecation was shown in *Caenorhabditis elegans* to activate a proton-gated ion channel in the adjacent muscle, thus showing that protons are an important transmitter in executing that motor program (8). Present results demonstrate the generality of this finding by documenting protonergic neural transmission in the inner ear.

The inner ear vestibular sensory epithelia of reptiles, birds, and mammals contain two hair cell types, I and II (both presynaptic to primary afferent processes) (9). Chalice-shaped terminals envelop one or more type I hair cells, forming synaptic contacts with the inner leaflet of the calyx terminal. Type II cells innervate bouton terminals and in some cases, the outer leaflets of calyces (10, 11). Synaptic transmission between type II cells and their terminals is chemically mediated and quantal (12, 13). Synaptic transmission between type I cells and their calyces has a quantal glutamatergic component (13–17) augmented by a nonquantal excitatory postsynaptic current (nqEPSC) (14, 16). It was hypothesized previously that the ball-and-socket morphology of the hair cell–calyx terminal might lead to the nqEPSC through stimulus-evoked modulation of the $[K^+]$ within the synaptic cleft (18–20). Present results support an alternative protonergic signaling mechanism, in which stimulus-evoked acidification of the cleft leads to modulation of a postsynaptic cationic conductance.

Results

Whole-cell voltage-clamp recordings from calyx nerve terminals in the vestibular lagena revealed slowly developing nqEPSCs and quantal excitatory postsynaptic currents (EPSCs) evoked by deflection of a single type I hair cell bundle (−60 mV hold). The experimental setup is illustrated in Fig. 1. For fluid jet mechanical stimuli, the bundle moved with a time constant of ~29 ms and reached an ~1-µm displacement within 20 ms of the stimulus onset, and for stiff-probe stimuli, it reached an ~1-µm displacement within 2 ms. Whole-cell capacitance averaged 27.3 pF (SD = 9.05) and series resistance averaged 38.0 MΩ (SD = 8.12). Pipette resistance was nominally 6 MΩ. In a majority of calyces (n = 36; 70%), deflection of a single hair cell bundle evoked a tonic nqEPSC without changing the rate of quantal EPSCs (Fig. 2A). In seven calyces (14%), bundle deflection evoked an increase in the rate of quantal EPSCs without evoking an nqEPSC (Fig. 2B), and in eight calyces (16%), bundle deflection simultaneously evoked an nqEPSC and an increased rate of quantal EPSCs (Fig. 2C). The EPSC rate adaptation time constant averaged 899 ms (115 ms minimum and 2,760 ms maximum; n = 9), excluding one cell that did not exhibit measureable adaptation. nqEPSCs did not adapt. This contrast is most easily seen in Fig. 2C, where the rate of quantal release declined during bundle deflection, whereas the nqEPSC reached a tonic plateau. nqEPSCs, therefore, offer an advantage over quantal EPSCs for conveying tonic or slowly changing signals. Quantal and nonquantal currents could be evoked simultaneously by deflection of a single hair bundle (Fig. 2C). A single hair cell is capable of conveying tonic depolarization through the nqEPSC and phasic information by adapting quantal release. This signaling implies the presence of a mechanism to adapt the rate of presynaptic vesicle release that does not interfere with

Significance

Recent evidence from the neuromuscular junction in *Drosophila* and *C. elegans* shows that protons are important intercellular signaling molecules operating to modulate presynaptic release or ion channels in adjacent cells. Here, we present evidence that protons also act directly as a nonquantal neurotransmitter in a contemporary amniote to convey excitatory stimuli from type I inner ear vestibular hair cells to their partner postsynaptic calyx nerve terminals. Protonergic neurotransmission works in concert with classical mechanisms and endows this system with a metabolically efficient mechanism to evoke tonic depolarizations of the postsynaptic neuron. Similar intercellular proton signaling mechanisms might be at play in the CNS.
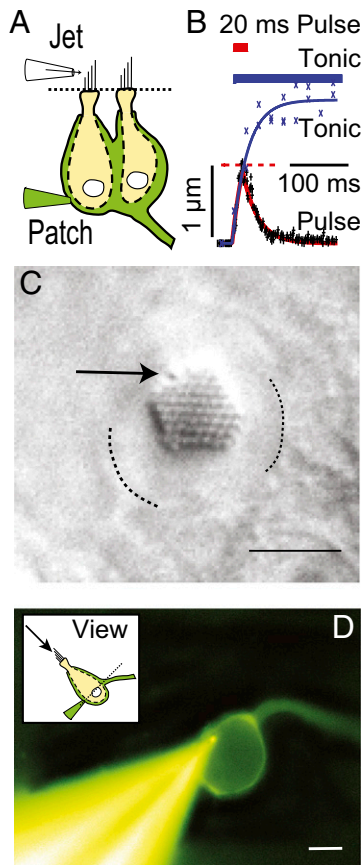
Fig. 1. Experimental setup. (*A*) Calyx terminal (green) in whole-cell voltage clamp (Patch) enveloping two type I hair cells (yellow). (*B*) In most experiments, a fluid jet was used to deflect the bundle > 1 μm within 20 ms of the stimulus onset and reached a plateau for tonic fluid jet stimuli with a time constant of $\tau_{RISE} = 29$ ms. (*C*) Differential interference contrast (DIC) image revealing the stereocilia and kinocilium (arrow). Apical border of the cell is indicated by dotted lines. (Scale bar: 5 μm.) (*D*) Fluorescence image of a Lucifer yellow-filled calyx and patch pipette. The axon is continuous with the calyx intracellular space and exits the panel on the right. (Scale bar: 7 μm.)

the plateau) shows that the nqEPSC was not caused by a buildup of the charge carrier(s) in the cleft. To confirm dependence on a change in membrane conductance, we recorded whole-cell resistance using a 256-Hz interrogating sine wave superimposed on the voltage-clamp command (Fig. 3*C*) (*n* = 3). Kinetics and magnitude of the conductance change were sufficient to explain the nqEPSC without any change in the electrochemical
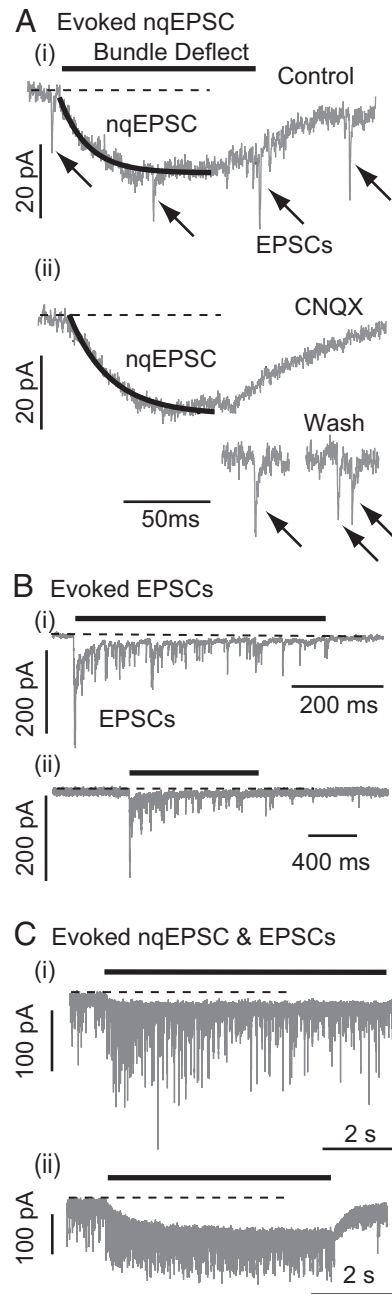

Fig. 2. nqEPSCs and EPSCs. (*A*, *i*) Recordings from a calyx expressing spontaneous EPSCs (arrows) and stimulus-evoked nqEPSCs (solid trace). (*A*, *ii*) CNQX reversibly eliminated quantal EPSCs but had no effect on nqEPSCs (14). (*B*) Evoked EPSCs recorded from (*i* and *ii*) two calyces showing adaptation of quantal release rates in response to deflection of a single hair bundle. The total current in these cells could be accounted for by a superposition of quantal events (32). (*C*) Example recordings from (*i* and *ii*) two calyces, where deflection of a single hair bundle simultaneously evoked nqEPSCs and quantal EPSCs. Note that the rate of quantal release adapted over time, whereas in the same cells, the nqEPSC developed to a plateau.

tonic nonquantal neurotransmission. Application of 6-cyano-7-nitroquinoxaline-2,3-dione (CNQX; 50 μM) reversibly blocked EPSCs but did not alter nqEPSC amplitude or kinetics (Fig. 2*A*) (*n* = 2), confirming a previous report showing that nqEPSCs were completely independent of glutamate receptor action (14). The origin of the nqEPSCs is the focus of the present report.

The amplitude of the nqEPSC for saturating stimuli was 106.2 pA (SE = 9.04 pA, −60 mV hold; *n* = 41). In 10 mM *4-(2-hydroxyethyl)-1-piperazineethanesulfonic acid* (Hepes) buffered media, the average rise time was $\tau_{on} = 436$ ms (SE = 40 ms), and decay time was $\tau_{off} = 318$ ms (SE = 44 ms). nqEPSC time constants were not limited by the 29-ms time constant of the fluid jet-driven hair bundle displacements. Fig. 3 *A* and *B* report the voltage sensitivity of the nqEPSC. The reversal potential shifted from +44 to +15 mV in these cells when *N*-methyl-D-glucamine (NMDG+) replaced media Na+ and on average, shifted from +36 to +6 mV (*n* = 5; average whole-cell *C* = 24.8 pF, *R* = 52.8 MΩ, electrode $R_E = 5.6$ MΩ). Reducing media [Ca²⁺] from 2.8 to 0.1 mM had no effect on the nqEPSCs. The time constant was not sensitive to the holding potential, with the exception of a singularity that occurred near the reversal potential, which would be expected if the channel is not perfectly selective for a single ion. The fact that the current reversed monotonically (i.e., the rising and falling phases reversed at the same potentials as
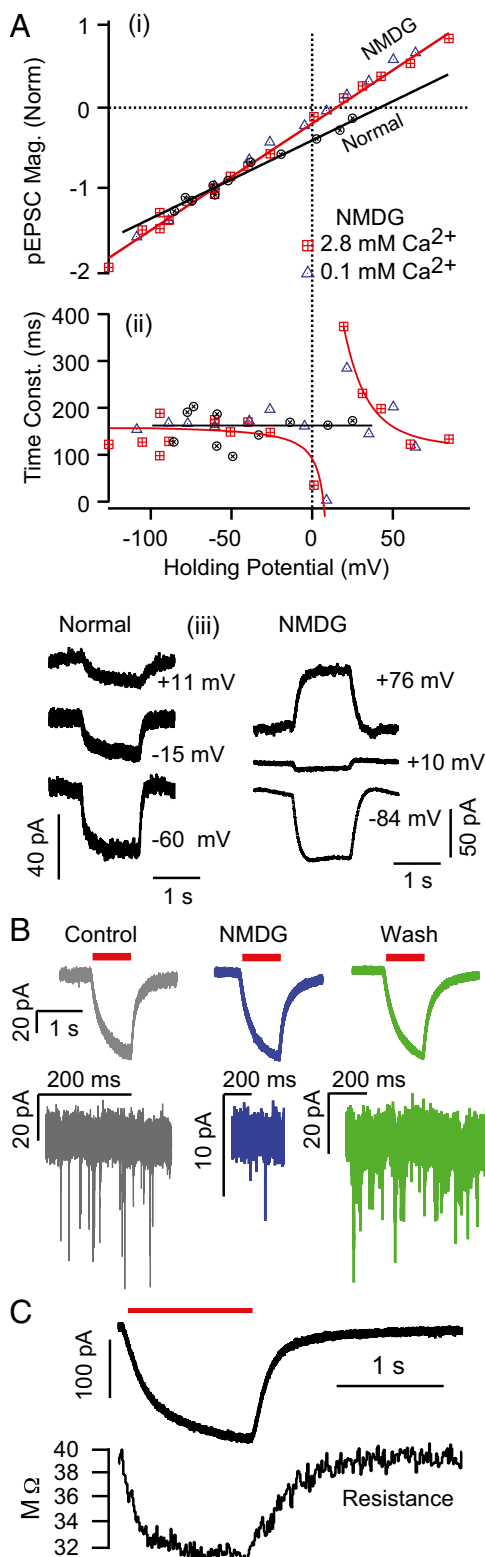
Highstein et al.

www.manaraa.com

Fig. 3. nqEPSC properties. (*A*, *i*) nqEPSCs reversed at +44 mV in control media and +15 mV when Na$^+$ was replaced by NMDG in the bath. Magnitudes were normalized to one at a holding potential of −60 mV to facilitate comparisons across cells. Reducing extracellular [Ca^{2+}] to 0.1 mM had no effect on the amplitude or reversal of nqEPSCs. (*A*, *ii*) nqEPSCs developed with time constants that were insensitive to [Na$^+$] and [Ca^{2+}] in the bath. Time constants were also insensitive to the holding potential, with the exception of voltages near the reversal potential. (*A*, *iii*) Sample nqEPSCs in normal media and NMDG. (*B*) Voltage-clamp recordings from a single calyx

potential during the stimulus. Data strongly suggest a stimulus-evoked chemical neurotransmitter released by hair cells into the cleft, leading to gating of a cation conductance.

To estimate charge carrier concentrations in the cleft, we used the known patch pipette solution and zero current potentials measured in *N*-(Dithiocarboxy)-*N*-methyl-D-glucamine sodium salt monohydrate (NMDG) and control media. Because we were unable to alter the nqEPSC with low extracellular [Ca^{2+}] (Fig. 3*A*), we assumed the current was carried primarily by Na$^+$ and K$^+$. Numerical optimization of Goldman–Hodgkin–Katz parameters (*SI Text*) estimated a relative permeability of $P_{Na/K} = 5.2$, $[K^+]_{CLEFT} = 84$ mM, and $[Na^+]_{CLEFT} = 41$ mM in normal media as well as $[K^+]_{CLEFT}^{NMDG} = 115$ mM and $[Na^+]_{CLEFT}^{NMDG} = 10$ mM in the presence of NMDG. These values reproduce the voltage sensitivity reported in Fig. 3 and indicate that the nqEPSC is driven, in part, by unusually high extracellular [K$^+$] and low [Na$^+$] in the cleft.

The relatively slow onset of the nqEPSC suggested that a stimulus-evoked signaling molecule might build up in the cleft and modulate the nqEPSC. Because increased metabolic activity leads to proton extrusion from hair cells, we examined changes in cleft pH as a candidate signal during hair bundle deflections. Fig. 4 ($n = 6$) illustrates the magnitude (Fig. 4*A*) and kinetics (Fig. 4*B*) of stimulus-evoked pH changes in the cleft. The hair bundle was imaged under control and stimulated conditions to quantify the stimulus (Fig. 4*A*, *i–iii*) (∼1 μm). Focusing down ∼12 μm below the cuticular plate revealed regions of high ratiometric membrane impermanent carboxylic acid, acetate, succinimidyl ester (SNARF, Life Technologies) concentration in the extracellular space around the hair cell. The fluorescent region was much larger than the extracellular synaptic cleft, presumably because of the 3D morphology, dye outside the calyx, and out-of-focus light (>5-μm optical slice). Ratiometric imaging was used to estimate the spatial distribution of pH in the control (Fig. 4*A*, *vii*) and stimulated (Fig. 4*A*, *viii*) conditions. The difference between the two provided acidification of the cleft. Punctate regions of high acidification (Fig. 4*A*, *ix*) were visible, suggesting that proton extrusion from hair cells might be spatially localized. For this specific cell, cleft acidification averaged ΔpH = −0.19 (−0.21 at puncta), and cleft acidification over all tested cells averaged ΔpH = −0.20 ($n = 4$, peak change at puncta, SD = 0.046). Because the highest ΔpH always occurred around the stimulated hair cell and not around other hair cells enveloped by the same calyx, we concluded that the stimulated hair cell was the source of protons entering the cleft.

Time-resolved confocal microscopy (21) was used to examine the kinetics of cleft acidification ($n = 3$). Fig. 4*B*, *i* provides the spatially averaged ΔF/F in the cleft surrounding stimulated hair cell 1 (green squares, Fig. S1). Imaging limitations likely account for the inability to resolve ΔpH puncta using this system and the small modulation in the center of hair cell 2 (black circles). We also analyzed ΔF/F in the Fourier domain to find the amplitude (Fig. 4*B*, *ii*) and phase (Fig. 4*B*, *iii*) (delay to peak ΔF/F) as functions of cleft position. The size of each symbol denotes the magnitude of modulation or relative delay for the region (∼1 μm²) of the image directly under the symbol. Stimulus-evoked cleft acidification was largest in the ring surrounding the stimulated hair cell and declined as the distance from the stimulated cell increased (Movie S1). Peak modulation was delayed ∼430 ms in distant regions relative to those adjacent to the stimulated hair cell. Results show injection of protons from the stimulated hair cell into the cleft, effective

held at −60 mV showing the reversible reduction of quantal EPSCs with little change in the nqEPSC in NMDG (blue traces). (*C*) nqEPSC was caused by a change in conductance.
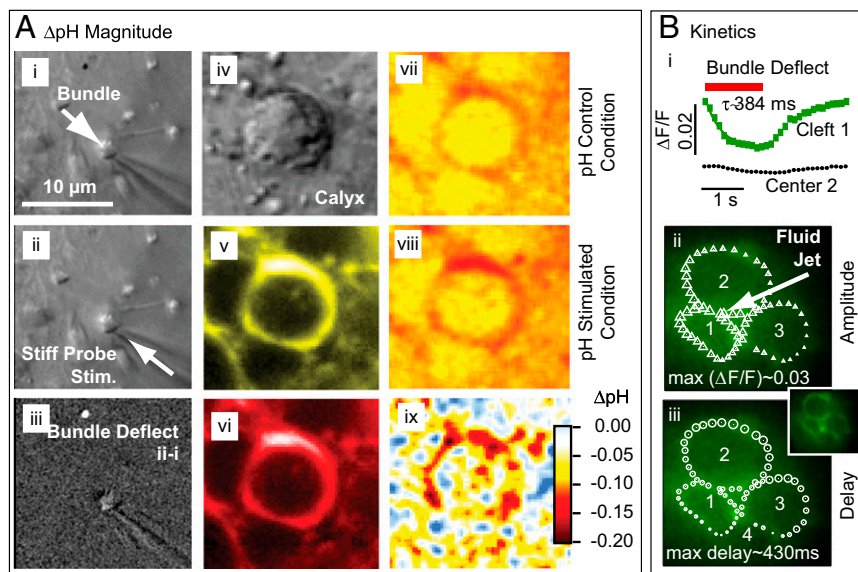
Fig. 4. Stimulus-evoked acidification of the synaptic cleft. (*A*) Magnitude of ΔpH determined by SNARF ratiometric imaging (*n* = 5). DIC image of hair bundle (*i*) in control condition, (*ii*) in deflected position, and (*iii*) subtraction (*ii* − *i*). (*iv*) DIC image of the calyx ~12 μm below the hair bundle and SNARF fluorescence emission in the extracellular space in the (*v*) yellow and (*vi*) red detection bands. Calibrated pH images under (*vii*) control, and (*viii*) bundle deflected conditions. (*ix*) Stimulus evoked acidification of the cleft (ΔpH *viii* − *vi*). (*B*) Kinetics of ΔpH determined by time-resolved impermanent indicator pyrannine H348 Δ*F/F* imaging (*n* = 3). (*i*) Time course of Δ*F/F* in the cleft around cell 1 and in a control location (center of cell 2). (*ii*) Symbol sizes show the first harmonic amplitude modulation of Δ*F/F* for repeated bundle deflections and (*iii*) relative time delay of peak Δ*F/F* as a function of position in the cleft. Results show that the largest pH changes occurred around the stimulated hair cell, whereas changes in remote regions of the calyx were smaller and time-delayed.

diffusion of protons away from the stimulated hair cell, and cycle-by-cycle clearance of protons.

The onset time constant of cleft acidification averaged 558 ms (*n* = 5, SD = 49) and was well within the range of the nqEPSC onset time constants recorded in the calyx [436 ms in 10 mM Hepes and 697 ms in 20 mM piperazine-*N,N*′-bis(2-ethanesulfonic acid) (PIPES)] This correlation led us to hypothesize that protons themselves might be the neurotransmitter leading to modulation of nqEPSCs, through direct (Fig. S2) or indirect action on a postsynaptic cation channel. If true, nqEPSC kinetics would be sensitive to pH buffering. To explore pH sensitivity, we modeled the cleft using a single compartment as illustrated in Fig. 5*A*. We assumed that protons were extruded from hair cells into the cleft at a stimulus-dependent rate $q(t)$ and buffered by a reversible second-order reaction within cleft volume V. Cleft pH homeostasis was modeled using a proportional mechanism driving free $[H^+]$ to baseline $[H]_0$ with gain k. For quasiequilibrium buffering, mass balance yields the model in Fig. 5*A*, where $[B]_0$ is the total concentration of bound and unbound buffer in the cleft, and K_d is the proton–buffer dissociation constant. Free proton concentration $[H^+]$ predicted by this model was used to drive a model of a ligand-gated ion channel (*SI Text*) to simulate nqEPSC kinetics (Fig. 5*B*, *i*).

Based on this analysis, increasing the strength of the buffer is predicted to slow the nqEPSC kinetics but not change the steady-state amplitude caused by proton homeostasis in the cleft. To test this prediction, we applied a series of extracellular pH buffers, all adjusted to a common pH, and recorded nqEPSC kinetics in control (10 mM Hepes, *n* = 37), test (1 mM Hepes, *n* = 8; 20 mM PIPES, *n* = 29), and then washout control conditions for individual cells. Time constants of the nqEPSC onset (τ_{ON}) and recovery (τ_{OFF}) in the control condition (10 mM Hepes) were used to define a characteristic nqEPSC time constant of each cell [$\tau_c = (\tau_{ON} + \tau_{OFF})/2$] (Fig. 5*B*). Results for each cell were normalized by τ_c to compensate for differences in calyx size (note V in Fig. 5*A* and morphological diversity Fig. S3). Application of 1 mM Hepes (pK ~ 7.4) significantly decreased the time constants,

whereas 20 mM PIPES (pK ~ 6.8) significantly increased them (*n* = 5, *P* < 0.001). All changes reversed with washout. Consistent with the data, the model predicted that PIPES should increase the time constant ~1.7-fold over the control buffer. These results show that nqEPSC is causally linked to free $[H^+]$ in the cleft.

Discussion

The vestibular calyx nerve ending is unique in the extent to which it envelops its presynaptic partners. This morphology maximizes the ability of the calyx to capture molecules exiting hair cells. Present results document capture of protons and modulation of a nonquantal postsynaptic cationic current in the vestibular calyx synaptic terminal. The strongest evidence for causal protonergic neurotransmission is the predictable effect of extracellular pH buffers on the kinetics of nqEPSCs (Fig. 5). It has been shown previously that stimulus-evoked acidification modulates quantal synaptic transmission through action on both Ca²⁺-dependent and -independent vesicular release pathways (22). This dependency raises the possibility that stimulus-evoked acidification of the cleft might also be linked to a protonergic feedback signal influencing quantal release and adaptation (23). Results support the general conclusions that protons serve as important intercellular transmitters (8) and synaptic signaling molecules (22, 23).

Because nqEPSCs were often present in the absence of quantal release (Fig. 2), and because puncta of high ΔpH were observed at locations distant from sites of quantal release (Fig. 4), we can rule out synaptic vesicles as the primary source of cleft acidification (24, 25). It is more likely that protons were extruded into the cleft during hair cell depolarization through mechanisms such as Na⁺/H⁺ exchange or electrogenic Na⁺/HCO₃ cotransport. The identity of the postsynaptic channel is unknown, and present results cannot distinguish whether the nqEPSC was directly gated by protons or a second messenger. It is likely that proton-sensitive ion channels are present in vestibular calyx terminals (*SI Text*, Fig. S2), but the extent to which they may contribute to the nqEPSC is not yet known.

A Kinetic Model of Cleft pH
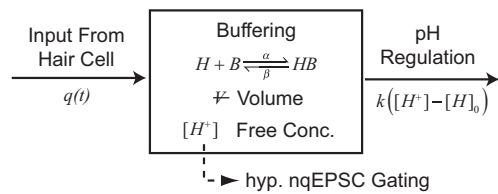
(Eq. 1)

$$\frac{d}{dt}\left\{[H^+]\left(1+\frac{[B]_0}{[H^+]+K_d}\right)\right\}=\frac{q}{V}-\frac{k}{V}\left([H^+]-[H]_0\right)$$

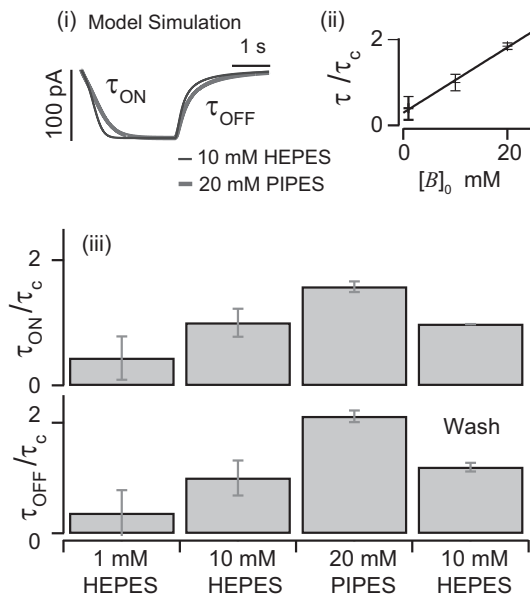## B nqEPSC Time Constant with Buffers

Fig. 5. Kinetics of cleft acidification were altered by pH buffers. (A) Single compartment model of the cleft accounting for stimulus-evoked proton input from the hair cell, reversible pH buffering within the cleft, and pH regulation by endogenous mechanisms. Buffering was assumed to be fast and in quasiequilibrium. (B) Exogenous buffers alter kinetics of nqEPSCs. (i) The model predicted that increasing buffer concentration would slow the speed of cleft acidification (because of buffer concentration $[B]_0$ and K_d) with no change in steady-state magnitude caused by endogenous pH regulation. (ii) Consistent with this model, nqEPSC onset (τ_{ON}), recovery time constants (τ_{OFF}), and average time constants $[\tau=(\tau_{ON}+\tau_{OFF})/2]$ increased with pH buffer strength ($n = 4$). Time constants were normalized for each cell by $\tau_c = \tau$ recorded in the same cell using 10 mM Hepes. (iii) Onset and recovery time constants both increased with the strength of the buffer and returned to control values on wash to 10 mM Hepes ($P < 0.05$, $n = 4$, average of 6–29 records/cell, error bars show SD of τ/τ_c between cells).

Present results suggest that the nqEPSC is carried by Na^+ and K^+ with a relative permeability of $\sim P_{Na/K} = 5.2$. Voltage sensitivity of the nqEPSC indicated that resting $[K^+]$ was maintained at an unusually high level in the cleft. It is likely that high cleft $[K^+]$ is facilitated by stimulus-evoked K^+ currents from hair cells (19, 20) and the low voltage-activating K^+ current present only in type I hair cells (26). Ionic homeostasis in the cleft is, therefore, critical and likely to be executed in part by the complex spatial array of channel proteins expressed in the calyx (27).

The $[H^+]$ transients evoked in remote regions of the cleft were delayed relative to transients around the stimulated hair cell. The delay suggests an effective proton diffusion coefficient of

$\sim 1.5 \times 10^{-5}$ cm^2 s^{-1} ($D \approx length^2/delay$). This parameter is not a classical diffusion coefficient because it includes effects of pH buffers and proton homeostasis. We estimate that 10 mM Hepes retarded the buildup of $[H^+]$ in the cleft and slowed the nqEPSCs at least threefold relative to endogenous conditions (Fig. 5) (asymptote with zero exogenous buffer), giving physiological estimates for the nqEPSC time constants of $\tau_{ON} \leq 145$ ms and $\tau_{OFF} \leq 106$ ms. Results also suggest that the effective proton diffusion coefficient in the cleft under physiological conditions is $\sim 4.5 \times 10^{-5}$ cm^2 s^{-1} or higher. This effective diffusion coefficient is very fast (like a shot) relative to proton diffusion in other systems (28) and implies that endogenous proton buffering is weak. Our findings also raise the possibility that the morphology of the cleft enhances long-range proton migration through the interaction between hydrated protons and the tightly juxtaposed membranes (29–31). Results show the importance of both morphology and endogenous pH buffering in determining pH kinetics in the cleft. nqEPSCs recorded in utricular calyces of immature rats (16) are considerably faster than in the adult turtle lagenar calyces examined here. The relatively small volume of the calyx synaptic cleft in young rats clearly would increase the speed of proton buildup relative to the turtle lagena (Fig. 5), accounting for at least some of the interspecies differences in nqEPSC kinetics.

Because protons are a byproduct of glycolytic metabolism and ATP hydrolysis, extrusion of protons by hair cells and capture by the calyx ending would constitute an energetically efficient mechanism for signaling tonic hair cell activation, whereas vesicular release would signal transient activation at a higher energetic cost. This energy efficiency may explain why nqEPSCs and calyx terminals are prolific in modern vestibular hair cell organs responsible for sensing tonic signals such as gravity, but absent from auditory hair cell organs responsible for sensing fast transient signals (12, 32).

Materials and Methods

Procedures complied with the Institutional Animal Care and Use Committee regulations at the Marine Biological Laboratory. Electrophysiological and imaging data were obtained from lagena of adult red-eared slider turtles, *Trachemys scripta elegans*. The otolithic membrane and otoconia were removed by incubation in type XXIV proteinase (0.06 mg·mL^{-1} in 0.1 mM calcium Ringer's solution; P8038; Sigma-Aldrich). Epithelia were superfused with an oxygenated Ringer's solution: 125 mM NaCl, 4 mM KCl, 2.2 mM MgCl$_2$, 2.8 mM CaCl$_2$, 8 mM D-glucose, and 1–10 mM Na-Hepes. Alternatively, 20 mM PIPES buffer was substituted for Hepes. NMDG+ was substituted for Na in some experiments. All extracellular solutions were pH-balanced to 7.53. CNQX (C$_9$H$_4$N$_4$O$_4$) was bath-applied (50 μM). Bath perfusion was continuous at 3 mL·min^{-1}.

Patch electrodes contained 120 mM KCl, 2.8 mM MgCl$_2$, 0.45 mM CaCl$_2$, 5 mM EGTA, 2.5 mM Na$_2$ATP, and 10 mM K–Hepes (pH 7.2) often in a 2–4% by weight solution of Lucifer yellow (Sigma-Aldrich) or 125 mM CsCl, 2.8 mM MgCl$_2$, 5 mM EGTA, 0.45 mM CaCl$_2$, 5 mM Hepes, and 2.5 mM NaATP (pH 7.5). Experiments were performed using a 63×, 1.0-N.A. objective on a fixed-stage Zeiss Axioskop FSII equipped with a swept field confocal (Prairie Technologies). Experimental protocols were computer-controlled (PatchMaster; HEKA). An Axon 700b amplifier (Molecular Devices) was used for whole-cell recording. Analog signals were recorded at 16 bits, filtered at 16 kHz (npi electronic GmbH), and sampled at 96 kHz (Apogee AD16x modified for DC coupling; IGOR Pro; Wavemetrics). Whole-cell capacitance was compensated online, and series resistance was compensated offline (*SI Text*).

Hair cell bundles were stimulated with a fluid jet attached to a picospritzer (1A; pv 800; WPI) or in a subset of experiments, by a closed-loop displacement-controlled stiff glass probe (P-841.3; Physick Instrumente). For fluid jet stimuli, the magnitude of the bundle movement, rise time, and delay relative to the electrical trigger were determined in a subset of experiments by recording the bundle motion with a CCD camera (Qimaging; Rolera MXi) and an image registration method (33, 34). The mechanical stimulus was set to achieve a maximum amplitude plateau nqEPSC.

Time-resolved confocal microscopy (21) was used to examine the kinetics and spatial distribution of cleft acidification. The membrane impermeable indicator pyranine H348 (HPTS; pK ~ 7.2, 20 μM; Invitrogen) was used; 500

Highstein et al.

swept field images (488 nm excitation, z488/568; Chroma Technology Detection) were collected at 2.5 frames s^{-1} (Prarie, 63× 0.9 w; Zeiss Axioskop) while repeating stimuli at 0.2 or 0.3 s^{-1}. The spatially averaged fluorescence was fit with an exponential decay. The deviation away from the exponential provided ΔF, and the value on the exponential provided F. Custom software time-stamped each pixel with the latency relative to the most recent stimulus trigger (21). Image data were analyzed using 1-μm^2 regions of interest (areas). A fluid jet stimulus was applied for ~50 periodic cycles, and Fourier analysis was applied.

To quantify the magnitude of pH changes, ratiometric membrane impermeant carboxy SNARF (pK ~ 7.5, 13 μM; Life Technologies) was used. A stiff glass probe was positioned to deflect a single hair bundle ~1 μm in the excitatory direction using a 1-Hz square wave periodic stimulus. Images of the bundle and extracellular fluorescence around the stimulated

hair cell (597- to 630-nm and 640- to 660-nm bands) were recorded using a dwell time of 1.64 ms pixel^{-1} (12 bit, 64 × 64 pixels) averaged over 6 min of acquisition (LSM 510; Zeiss Confocal). Ratiometric fluorescence was calibrated to estimate pH using pH standards (6.8–7.51) in the bath. The change, ΔpH, was estimated by subtracting the stimulated condition from the control condition and corrected for the 50% duty cycle of the square wave stimulus.

1. De Robertis ED, Bennett HS (1955) Some features of the submicroscopic morphology of synapses in frog and earthworm. *J Biophys Biochem Cytol* 1(1):47–58.
2. Whittaker VP, Gray EG (1962) The synapse: Biology and morphology. *Br Med Bull* 18:223–228.
3. Ignarro LJ, Buga GM, Wood KS, Byrns RE, Chaudhuri G (1987) Endothelium-derived relaxing factor produced and released from artery and vein is nitric oxide. *Proc Natl Acad Sci USA* 84(24):9265–9269.
4. Gillman MA, Lichtigfeld FJ (1994) NO comments. *Nature* 367(6458):28.
5. Barañano DE, Ferris CD, Snyder SH (2001) Atypical neural messengers. *Trends Neurosci* 24(2):99–106.
6. Katz B, Schmitt OH (1940) Electric interaction between two adjacent nerve fibres. *J Physiol* 97(4):471–488.
7. Furshpan EJ, Potter DD (1957) Mechanism of nerve-impulse transmission at a crayfish synapse. *Nature* 180(4581):342–343.
8. Beg AA, Ernstrom GG, Nix P, Davis MW, Jorgensen EM (2008) Protons act as a transmitter for muscle contraction in C. elegans. *Cell* 132(1):149–160.
9. Wersall J (1956) Studies on the structure and innervation of the sensory epithelium of the cristae ampullares in the guinea pig: A light and electron microscopic investigation. *Acta Otolaryngol Suppl* 126(1956):1–85.
10. Gulley RL, Bagger-Sjöbäck D (1979) Freeze-fracture studies on the synapse between the type I hair cell and the calyceal terminal in the guinea-pig vestibular system. *J Neurocytol* 8(5):591–603.
11. Hamilton DW (1968) The calyceal synapse of type I vestibular hair cells. *J Ultrastruct Res* 23(1):98–114.
12. Furukawa T, Ishii Y, Matsuura S (1972) Synaptic delay and time course of postsynaptic potentials at the junction between hair cells and eighth nerve fibers in the goldfish. *Jpn J Physiol* 22(6):617–635.
13. Schessel DA, Ginzberg R, Highstein SM (1991) Morphophysiology of synaptic transmission between type I hair cells and vestibular primary afferents. An intracellular study employing horseradish peroxidase in the lizard, Calotes versicolor. *Brain Res* 544(1):1–16.
14. Holt JC, Chatlani S, Lysakowski A, Goldberg JM (2007) Quantal and nonquantal transmission in calyx-bearing fibers of the turtle posterior crista. *J Neurophysiol* 98(3):1083–1101.
15. Bonsacquet J, Brugeaud A, Compan V, Desmadryl G, Chabbert C (2006) AMPA type glutamate receptor mediates neurotransmission at turtle vestibular calyx synapse. *J Physiol* 576(Pt 1):63–71.
16. Songer JE, Eatock RA (2013) Tuning and timing in mammalian type I hair cells and calyceal synapses. *J Neurosci* 33(8):3706–3724.
17. Rennie KJ, Streeter MA (2006) Voltage-dependent currents in isolated vestibular afferent calyx terminals. *J Neurophysiol* 95(1):26–32.
18. Goldberg JM (1996) Theoretical analysis of intercellular communication between the vestibular type I hair cell and its calyx ending. *J Neurophysiol* 76(3):1942–1957.
19. Lim R, Kindig AE, Donne SW, Callister RJ, Brichta AM (2011) Potassium accumulation between type I hair cells and calyx terminals in mouse crista. *Exp Brain Res* 210(3-4):607–621.
20. Contini D, et al. (2012) Intercellular K$^+$ accumulation depolarizes Type I vestibular hair cells and their associated afferent nerve calyx. *Neuroscience* 227:232–246.
21. Hakizimana P, Brownell WE, Jacob S, Fridberger A (2012) Sound-induced length changes in outer hair cell stereocilia. *Nat Commun* 3:1094.
22. Caldwell L, Harries P, Sydlik S, Schwiening CJ (2013) Presynaptic pH and vesicle fusion in Drosophila larvae neurones. *Synapse* 67(11):729–740.
23. Wang TM, Holzhausen LC, Kramer RH (2014) Imaging an optogenetic pH sensor reveals that protons mediate lateral inhibition in the retina. *Nat Neurosci* 17(2):262–268.
24. Palmer MJ, Hull C, Vigh J, von Gersdorff H (2003) Synaptic cleft acidification and modulation of short-term depression by exocytosed protons in retinal bipolar cells. *J Neurosci* 23(36):11332–11341.
25. Dalet A, et al. (2012) Glutamate transporters EAAT4 and EAAT5 are expressed in vestibular hair cells and calyx endings. *PLoS ONE* 7(9):e46261.
26. Hurley KM, et al. (2006) M-like K+ currents in type I hair cells and calyx afferent endings of the developing rat utricle. *J Neurosci* 26(40):10253–10269.
27. Lysakowski A, et al. (2011) Molecular microdomains in a sensory terminal, the vestibular calyx ending. *J Neurosci* 31(27):10101–10114.
28. Swietach P, Leem CH, Spitzer KW, Vaughan-Jones RD (2005) Experimental generation and computational modeling of intracellular pH gradients in cardiac myocytes. *Biophys J* 88(4):3018–3037.
29. Knight C, Voth GA (2012) The curious case of the hydrated proton. *Acc Chem Res* 45(1):101–109.
30. Alexiev U, Mollaaghababa R, Scherrer P, Khorana HG, Heyn MP (1995) Rapid long-range proton diffusion along the surface of the purple membrane and delayed proton transfer into the bulk. *Proc Natl Acad Sci USA* 92(2):372–376.
31. Heberle J, Riesle J, Thiedemann G, Oesterhelt D, Dencher NA (1994) Proton migration along the membrane surface and retarded surface to bulk transfer. *Nature* 370(6488):379–382.
32. Li GL, Keen E, Andor-Ardó D, Hudspeth AJ, von Gersdorff H (2009) The unitary event underlying multiquantal EPSCs at a hair cell's ribbon synapse. *J Neurosci* 29(23):7558–7568.
33. Rabbitt RD, Boyle R, Highstein SM (2010) Mechanical amplification by hair cells in the semicircular canals. *Proc Natl Acad Sci USA* 107(8):3864–3869.
34. Thévenaz P, Ruttimann UE, Unser M (1998) A pyramid approach to subpixel registration based on intensity. *IEEE Trans Image Process* 7(1):27–41.

www.manaraa.com